ISSN 1027-5495. Functional Materials, 28, No.2 (2021), p. 266-274.
doi:https://doi.org/10.15407/fm28.02.266

Transfer processes in an equiatomic FeNi composite obtained by electroconsolidation

***G.Ya.Khadzhai*[1], *S.R.Vovk*[2,3], *E.S.Gevorkyan*[1,2], *S.V.Dukarov*[1], *M.V.Kislitsa*[1], *A.Feher*[3], *V.N.Sukhov*[1], *R.V.Vovk*[1]**

[1]V. Karazin Kharkiv National University, 4 Svobody Sq., 61022 Kharkiv, Ukraine
[2]Ukrainian State University of Railway Transport, 7 Feierbakh Sq., 61050 Kharkiv, Ukraine
[3]Centre of Low Temperature Physics, Faculty of Science, P. Safarik University, 9 Park Angelinum, 04154 Kosice, Slovakia

Received October 11, 2020

The paper presents studying by resistive and energy-dispersive methods the transfer processes in a binary Fe–Ni system obtained by the method of electroconsolidation (SPS technology). Well-separated regions of almost pure iron and nickel were found. The concentration dependence of interdiffusion in the composite under study passes through a maximum at a nickel concentration of ~ 70 at. %. It is shown that the value of the interdiffusion coefficient of the electroconsolidated Fe–Ni composite is significantly higher than that of an alloy of similar composition, which is probably the result of the effect of the SPS technology, as well as an increase in the contribution of intergranular diffusion. It was found that the electrical and thermal conductivity of an electroconsolidated sample is significantly higher than that of samples of the same composition obtained by melting. It was found that the temperature dependences of the resistivity of the electroconsolidated sample in the investigated range of 5–300 K are due to the scattering of electrons by defects and phonons, and the scattering of electrons by phonons can be approximated with a high accuracy by the Bloch-Gruneisen-Wilson relation.

Keywords: electroconsolidation, interdiffusion, electrical conductivity, thermal conductivity, electrons, phonons, scattering, energy-dispersive methods.

Процеси переносу в еквіатомному композиті FeNi, отриманому електроконсолідацією. *Г.Я.Хаджай, С.Р.Вовк, Е.С.Геворкян, С.В.Дукаров, М.В.Кислиця, А.Фехер, В.Н.Сухов, Р.В.Вовк*

Представлено дослідження резистивним та енергодисперсійним методами процесів переносу у бінарній системі Fe–Ni, отриманій методом електроконсолідації (SPS-технологія). Виявлено добре розділені області майже чистого заліза і нікелю. Концентраційна залежність взаємної дифузії у дослідженому композиті проходить через максимум при концентрації нікелю ~ 70 at. %. Показано, що значення коефіцієнта взаємної дифузії електроконсолідованого композиту Fe–Ni значно вище, ніж у сплаві аналогічного складу, що, ймовірно, є результатом впливу технології SPS, а також збільшення внеску міжгранулярної дифузії. Встановлено, що електро- та теплопровідність електроконсолідованого зразка істотно вищі, ніж у зразків того ж складу, отриманих плавленням. Виявлено, що температурні залежності електроопору електроконсолідованого зразка у дослідженому інтервалі 5–300 K обумовлені розсіюванням електронів на дефектах та фононах, причому розсіювання електронів на фононах можна з високою точністю апроксимувати співвідношенням Блоха-Грюнайзена-Вільсона.

Представлено исследование резистивными и энергодисперсинными методами процессов переноса в бинарной системе Fe–Ni, полученной методом электроконсолидации (SPS-технология). Обнаружены хорошо разделенные области почти чистого железа и никеля. Концентрационная зависимость взаимной диффузии в исследованном композите проходит через максимум при концентрации никеля ~ 70 at. %. Показано, что значение коэффициента взаимной диффузии электроконсолидированного композита Fe–Ni значительно выше, чем у сплава аналогичного состава, что, вероятно, является результатом воздействия технологии SPS, а также увеличения вклада межграничной диффузии. Установлено, что электро- и теплопроводность электроконсолидированного образца существенно выше, чем у образцов того же состава, полученных плавлением. Обнаружено, что температурные зависимости электросопротивления электроконсолидированного образца в исследованном интервале 5–300 К обусловлены рассеянием электронов на дефектах и фононах, причем рассеяние электронов на фононах можно с высокой точностью аппроксимировать соотношением Блоха-Грюнайзена-Вильсона.

1. Introduction

The production of new materials for multifunctional materials purposes with specified magneto-resistive characteristics remains one of the main directions of modern solid state physics [1–5]. Notably, an important role in the development of technologies for obtaining such materials can be played by the use of intensive compaction methods such as electroconsolidation [6], special nanostructuring techniques [7], including the use of extreme external influences such as high pressures, irradiation with high-energy electrons [1, 8], as well as the use of modern methods of modeling their structure and technological characteristics [9, 10].

Binary metal systems are important in modern technologies and are widely used both in metallurgy and in specialized scientific applications. The system combines the availability of components and specific properties. Thus, this binary system is applied in modern technologies, for example, in matrices for OLED displays. This stimulates active research towards improving the methods of electrodeposition of this alloy [11, 12]. Composite structures based on are widely used as protective coatings [13] and as the base of catalysts in plastic processing [14, 15], water splitting [16–19], and hydrogen storage [20, 21]. It should be noted that, along with other bimetallic systems [22], is considered as a bifunctional element for oxygen release and reduction in fuel cells and zinc air batteries [23]. Highly ordered Fe–Ni alloys (so-called Tetrataenite) are considered as an affordable alternative to modern high-power magnets based on rare earth materials [24, 25].

Equiatomic magnetic nickel-iron alloys has an increased magnetic permeability, increased induction of technical saturation and a rectangular hysteresis loop, which is widely used in computers and automatic control devices [1]. Therefore, studies ai med at controlling the properties of such alloys, as well as improving the methods of their preparation [1, 6, 9, 10], seem to be very promising.

It should be noted that, despite the extensive development of various, primarily electrochemical, methods for obtaining structures based on, metallurgical methods, in particular sintering, remain the basis of many modern technologies.

Electroconsolidation technologies Field Activated Sintering Techniques (FAST) and Spark Plasma Sintering (SPS) [26] are very effective for the manufacture of composites of difficult-to-sinter materials and compounds. In such technologies, an electric current is passed in the direction of the applied external pressure, causing heating due to the field and direct influences. This makes it possible to significantly accelerate heating and reduce the sintering time to several minutes; since crystal grains large do not have time to grow, the compaction is ahead of grain growth [27] and a high-density and finely dispersed composite structure is provided [28].

During consolidation, mass transfer is activated by surface and volume diffusion, as well as plastic deformation [29]. These processes are activated by the temperature, which during electroconsolidation, lies in the range of $0.5T_{melt.} < T_{sint.} < T_{melt.}$. In the places of point contacts of the grains occurs their deformation, while the area of the boundaries increases many times, which increases the mass transfer. Electric discharge processes occur along the particle boundaries, which accelerates consolidation due to local welding of powder particles and additional mass transfer due to internal temperature gradients in the composite under the influence of inhomogeneous elec-

tric current density between the pores [30]. The local formation of plasma as a result of the action of electric discharges leads to cleaning and activation of the surface of the sintered powders, which significantly contributes to both the chemical purity of the final product and the compaction of the sintered powders [31].

At the same time, the diffusion processes occurring in the binary system, both during its formation and during operation, have not yet been sufficiently studied; although it is diffusion processes that ultimately determine not only the possibility of creating structures with specified functional properties, but also their preservation over time.

For such systems, it is of fundamental interest to study the transport properties, electrical and the thermal conductivity, especially at low temperatures, where the temperature dependence of electrical resistivity is caused by the scattering of electrons by phonons, defects, electrons and magnons, and the temperature dependence of thermal conductivity is determined, first of all, by the scattering of heat carriers — electrons and phonons — on defects and on each other.

In this work we present a study of the concentration dependence of the diffusion coefficient, as well as a study of electrical conductivity and thermal conductivity in the range of 4.2–300 K in metal composite samples obtained by the method of electroconsolidation (SPS).

2. Experimental

The samples were prepared by the method of electroconsolidation of nickel (PNE-45-200 μm, nickel content 99.9 %) and iron (pulverized PZhR 2.200.28, iron content 99.9 %) powders with a grain size of about 200 μm. The electroconsolidation was carried out for 10 min at 1100°C, a pressure of 35 MPa and a current of ~ 5 kA. The heating rate was ~ 200°C/min. The obtained composite sample had the shape of a rectangular bar with dimensions of 15×4×6 mm^3.

The surface of the sample was carefully polished and examined in a Tescan Vega 3LMH scanning electron microscope equipped with a Bruker XFlash 5010 EDS characteristic X-ray detector.

The determination of the elemental composition was carried out in the detector self-calibration mode. To determine the spatial distribution of the elements, the sample was scanned in a direction parallel or perpendicular to the direction of the electric current passing through the sample and the direction of the pressure applied during sintering. The spatial step of the probe during the transition from one scanning point to another was 1 or 2 μm, and the time of signal accumulation from one point was usually chosen equal to 32 s. For all elements, except iron and nickel, the "Deconvolution only" mode was selected. To take into account the possible influence of the shape of the initial particle and surface effects on the mass transfer of the substance, in a separate series of experiments, the successive passage of the electron probe along the same line of the sample was carried out using different values of the accelerating voltage. Since the penetration depth of electrons and, consequently , the region of generation of the characteristic X-ray radiation signal, strongly depend on the initial energy of electrons, this made it possible to gain some insight into the effect of the form factor on diffusion processes in the sample.

Sample resistivity, $\rho(T)$, was measured by the standard 4-contact method; thermal conductivity, $\lambda(T)$, was measured by the method of stationary uniaxial heat flow. The temperature range of measurements was 4.2–300 K.

3. Results and discussion

Fig. 1 shows the elemental distribution map and SEM image for a sample after sintering. It can be seen that the sample is two-phase, with clearly separated regions of almost pure iron and nickel. The contrast between the phases is well observed not only in BSE, but also in SE modes. This is possibly due to the different hardness of nickel and iron, which causes a morphological contrast when polished.

A typical dependence of the nickel (or iron) concentration on the probe coordinate is shown in Fig. 2. The left edge of the SEM image was taken as a reference point. The size of the frame and its location were chosen in such a way as to capture the regions of the phase zones free of the second component (see Fig. 3).

Fig. 4 shows the results of constructing the distribution of elements along the scanning line, obtained at different values of the accelerating voltage. Scanning was carried out along the same line, without moving the sample (see Fig. 3). Fig. 4 represents the distribution of elements over the depth of the sample. It can be seen that, in the central region of the distribution, the difference between the concentrations obtained at the

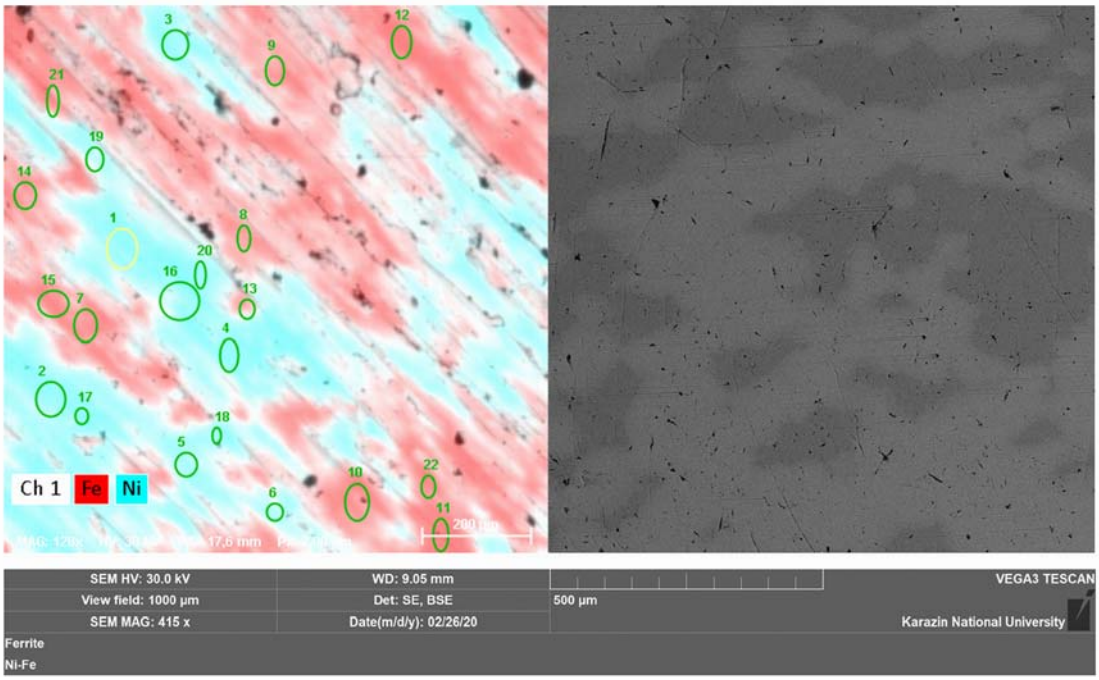

Fig. 1. Results of elemental mapping and SEM image of a Fe–Ni composite sample obtained by electroconsolidation.

same point of the sample at probe energies of 15 and 30 keV reaches 20–25 at.%. For comparison, note that at the same accelerating voltage for successive scanning cycles, the difference between the dependences is only 1–2 % and is random. The observed effect can be associated with the features of the distribution of the substance in a narrow layer on the grain surface, which can have a decisive influence on the behavior of nanocomposite structures. In the previous work [25] it was showed that due to the size dependence of the diffusion coefficient, the synthesis of functional structures of the FeNi phase of the L10 type is possible only at a temperature of 320°C. However, a detailed understanding of this phenomenon requires further work.

To obtain the concentration dependences of the diffusion coefficient, we used the data obtained at a probe energy of 30 keV. As it is seen from Fig. 4, with an increase in the probe energy, the experimental dependences asymptotically approach those obtained at an accelerating voltage of 30 kV. This characterizes the diffusion processes occurring in the bulk of the sintered material.

Applying the Boltzmann-Matano method to the $C_{Ni}(x)$ curve (Fig. 2), we calculated the concentration dependence of the mutual diffusion coefficient $\tilde{D}(C)$ [32]. The results are shown in Fig. 5. Note that we have not found a significant effect of the probe passage direction (relative to the direction of passage of the current applied during sintering) on the value of the diffusion coefficient.

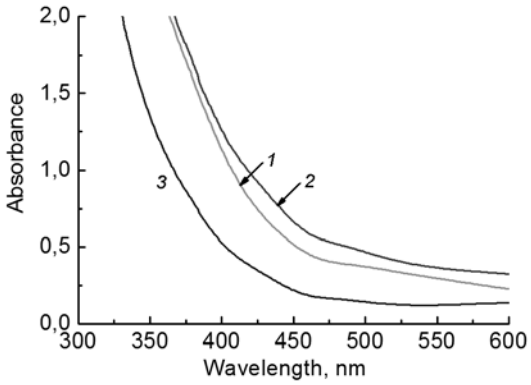

Fig. 2. Dependences of the nickel concentration on the coordinates along the scan line.

The dependence $\tilde{D}(C)$ has the form of a smooth curve with a maximum in the region of ~ 70 at.%. Ni, which is in accordance with the literature data (see, for example [33–36]) for the coefficient of mutual diffusion in the system and is interpreted as the concentration dependence of the diffusion coefficient of the components in the binary Fe–Ni alloy with unlimited solubility of the components. The maximum in the $\tilde{D}(C)$ dependence is associated with the shape of the

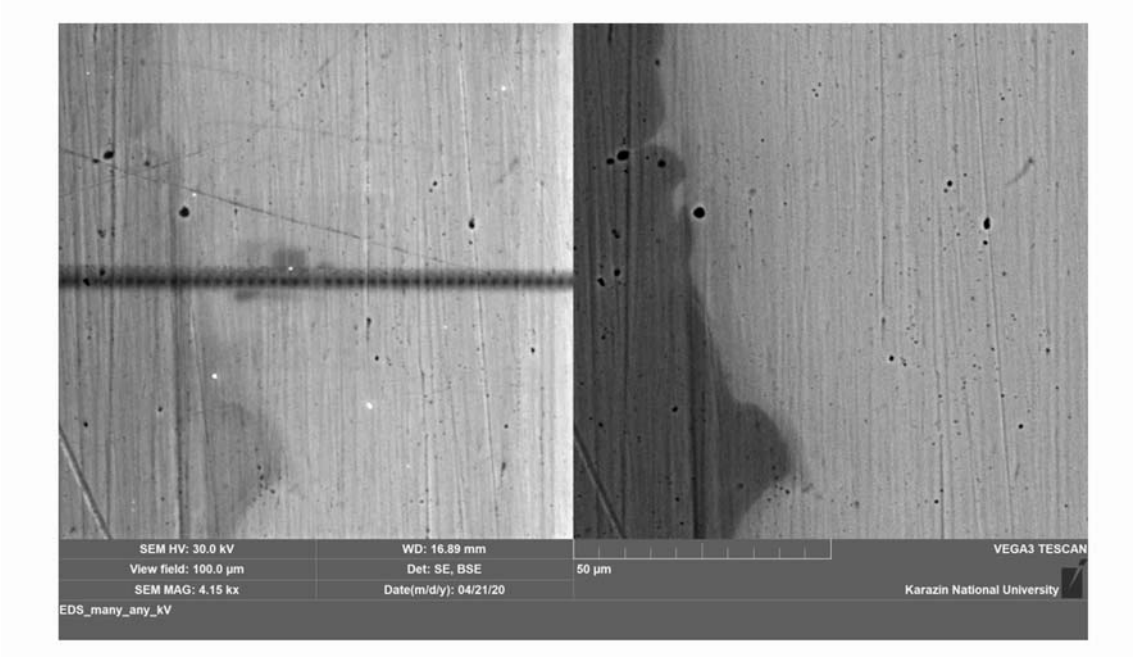

Fig. 3. An example of cropping to obtain a series of EDS spectra. The SE image shows the effects of carbon contamination stimulated by multiple passes of the electron beam.

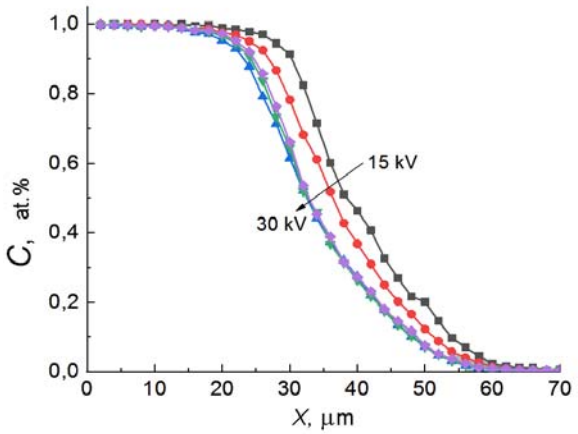

Fig. 4. Iron concentrations depending on the coordinate at different energies of the electron probe.

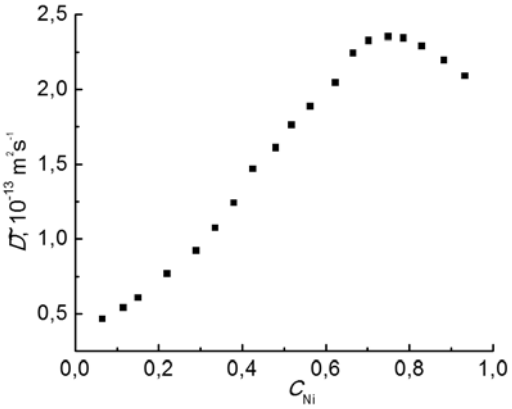

Fig. 5. Concentration dependence of the nickel diffusion coefficient $\tilde{D}(C_{Ni})$ in the Fe–Ni composite.

equilibrium diagram of the binary system, in which the liquidus and solidus curves for alloys with a Ni content of 5.9–100 at.% have the form of a sagging chain with a minimum at 1436°C and an atomic Ni concentration of 68 %.

It is known, that the lower the melting point of the alloy, the higher the diffusion mobility of atoms in an alloy with a variable concentration. That is why the coefficient of mutual diffusion of an alloy with a concentration of ~ 70 at.% Ni has the maximum value.

However, we obtain the values of the diffusion coefficient much higher than in the literature [33–36]. The higher values of the diffusion coefficients can be associated with the effect of electric current flowing through the Fe and Ni particles. The current causes local heating and cleaning of the particle surface. This activates the diffusion process. In addition, due to the large area of grain boundaries in composites, diffusion mass transfer along the boundaries can become decisive.

The experimental results of measurements of electrical resistivity and thermal conductivity are shown in Fig. 6. It is seen

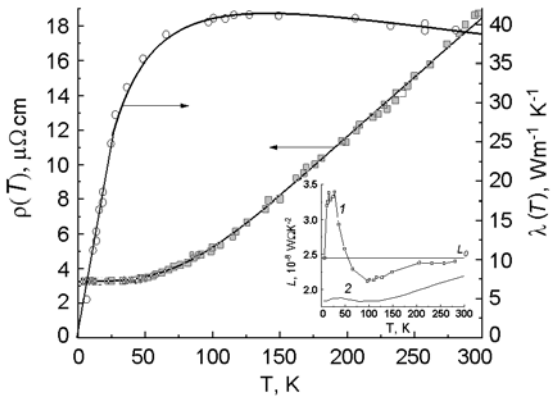

Fig. 6. Temperature dependences of electrical resistivity and thermal conductivity of electroconsolidated $Fe_{0.5}Ni_{0.5}$ alloy. □, O — the experimental curve for the electrical resistivity drawn in accordance with (1)–(2); the curve for thermal conductivity is drawn "by eye". In the inset, the Lorentz function, $L(T) = \lambda_e(e)\rho(T)/T$ is drawn: *1* — according to our data; *2* — according to [38, 39].

that in the region of residual resistance ($\rho(T) \approx \rho_0 \approx 3.26$ μΩcm, $T \leq 25$ K) the thermal conductivity is proportional to the temperature $\lambda_e(T) \sim T$. This behavior of both parameters indicates the transfer of heat by electrons, which, in this temperature range, is characterized by elastic scattering of electrons by impurities and other defects. In this case, the Wiedemann-Franz-Lorentz law is fulfilled: $\rho(T)\lambda_e(T)/T \approx \rho_0\lambda_e(T)/T \approx$ const [37].

At high temperatures $T \geq \theta$ (θ is the Debye temperature, see Table), elastic scattering of electrons by phonons prevails [37]. Here $\rho(T) \sim T$, $\lambda_e(T) \approx$ const, and the Wiedemann-Franz-Lorenz law also holds. However, as can be seen from Fig. 6, in our case, at the highest of the studied temperatures, the thermal conductivity does not yet reach a constant value, that is, the scattering of electrons by phonons still remains inelastic and $\lambda_e(T)\rho(T)/T = L(T) < L_0$ [37].

The behavior of the Lorentz function, $L(T)$, in the investigated temperature range is shown in the inset to Fig. 6 (curve *1*). The low-temperature maximum present in the $L(T)$ dependence was observed in previous studies [40, 41]. The inset to Fig. 6 (curve *2*) shows the Lorentz function constructed according to the recommended data for the system with a significantly higher residual resistance (14.8 μΩcm) [38, 39]. In this case, the $L(T)$ curve (inset, curve *2*) also exhibits a low-temperature maximum, but it is very weakly expressed. That is, the low-temperature maximum in $L(T)$ decreases with an increase in the defectiveness of the sample, while the contribution of phonons to the thermal conductivity of the alloys increases with an increase in the defectiveness [37, 42]. Thus, the maximum $L(T)$ is probably associated with the peculiarities of the electron scattering by impurities and the deformation of the phonon spectrum under the influence of the latter [43, 44].

Fig. 7 shows the electrical resistivity and the thermal conductivity of the electroconsolidated composite together with the data [38, 39, 45] for the alloy and the recommended data [38, 39] for Fe and Ni. The electroconsolidation parameters indicate that the investigated sample consists of Fe and Ni particles; therefore, it could be expected that both the resistivity and the thermal conductivity of the sample will lie between curves *2* and *3* in Fig. 7a and b (see, for example, [46, 47]).

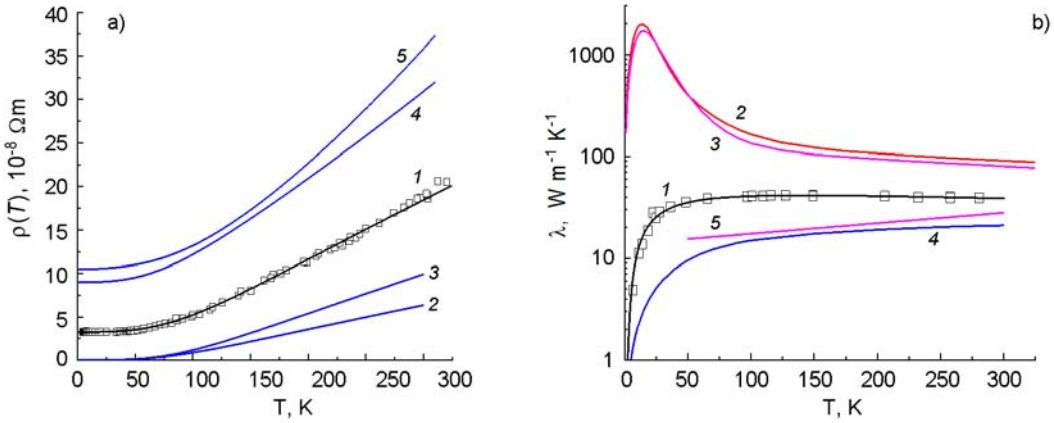

Fig. 7. Temperature dependences of electrical resistivity (a) and thermal conductivity (b). *1* — Fe–Ni composite; *2* — Ni [38–39]*, *3* — Fe [38–39]*, *4* — FeNi alloy [38, 39]*, *5* — FeNi alloy [45]*. * — the recommended values.

Table. The approximation parameters $\rho(T)$ in the range of 4.2–300 K for the equiatomic system FeNi, as well as Ni and Fe, by equations (1)–(2)

No.	Composition	$\rho_0 \cdot 10^8$ Ωcdot БШ sAvW% A pBm	$C_3 \cdot 10^8$ Ω·m	$C_5 \cdot 10^8$ Ω·m	θ, K	$b_0 \cdot 10^4$, Ω·m/K^2
1	Fe–Ni	3.26	75	0	624	0
2	FeNi [38]*	9	63	5.5	528	0.605
3	F2FeNi [45]	10.49	69	18.5	726	1.4
4	Fe [38]*	0.0225	22.4	47.9	587	0
5	Ni [38]*	0.0032	25.35	6.05	575	0.071

However, it is seen that the resistivity and the thermal conductivity of the composite (curves *1*) lie between the corresponding curves (*2* and *3*) obtained for the metals Fe and Ni, and for the alloy with a large value of residual resistance (curves 4 and 5). This means that grain boundaries in the composite restrict heat and charge fluxes to a lesser extent than disorder in the case of homogeneous alloys with the same ratio of components.

In the entire investigated temperature range of 4.2–300 K, the experimental results on the electrical resistivity of the electroconsolidated FeNi can be approximated with a high accuracy ($\Delta\rho/\rho \leq 1$ %) by the formula:

$$\rho(T) = \rho_0 + \rho_{ph} + b_0 \cdot T^2. \qquad (1)$$

Here ρ_0 is the residual resistance associated with the scattering of electrons by defects; ρ_{ph} is the resistivity due to the scattering of electrons by phonons. In general form, this term can be represented as [48 49]

$$\rho_{ph}(T) = \qquad (2)$$

$$= C_5\left(\frac{T}{\theta}\right)^5 \cdot \int_0^{\theta/T} \frac{e^x x^5 dx}{(e^x-1)^2} + C_3\left(\frac{T}{\theta}\right)^3 \cdot \int_0^{\theta/T} \frac{e^x x^3 dx}{(e^x-1)^2} \quad .$$

Moreover, the first term (the Bloch-Gruneisen relation) describes the intraband, *s–s* scattering of electrons, while the second term is related to the interband *s–d* scattering characteristic for the transition metals, their alloys and compounds [48–53]; x is the constant of integration.

The term $b_0 \cdot T^2$ is often associated with electron-electron scattering (see, for example, [54, 55]) or with the scattering of electrons by spin waves [45, 55]. In [55], it was noted that the experimental values of the coefficients b_0 for ferro- and non-ferromagnetic metals are close in magnitude. In [56–58], the term $b_0 \cdot T^2$ was associated with the interference between electron-phonon and electron-impurity interactions. In this case, the parameter b_0 increases with increasing defect concentration.

The Table shows the fitting parameters of equations (1)–(2) to the temperature dependence of the resistivity of the FeNi system for our sample, for the data [38] and [45], as well as for Fe and Ni [38].

It can be seen from Table 1 that in the investigated composites, the scattering of electrons by phonons is due to interband *s-d* transitions, while *s–s* scattering is absent: $C_5 = 0$. Electron-electron scattering and scattering of electrons by spin waves were also not found. The absence of the $b_0 \cdot T^2$ term most likely indicates a relatively small number of defects in the sample.

Differences in the parameters of approximation $\rho(T)$ for the Fe–Ni system and for the metals Fe and Ni are also seen. For the system, the parameters C_5 and b_0 increase with increasing ρ_0, that is, with increasing sample defectiveness. This behavior of the term $b_0 T^2$ indicates that this term is associated with the interference between inelastic scattering of electrons by phonons and elastic scattering of electrons at boundaries and defects [56–58]. An increase in the parameter C_5 with increasing ρ_0 is probably associated with the presence of heavy impurities [43] in the Fe–Ni system considered in [38, 45]. The values of the parameters C_3 are close to each other and do not depend on ρ_0.

As for the recommended values for Fe and Ni metals, they refer to materials of sufficiently high purity ($rrr_{Fe} \approx 440$ and $rrr_{Ni} \approx 1860$). For these data, the C_3 parameters are very close to each other, but about three times less than for the Fe–Ni system. The term $b_0 T^2$ turned out to be necessary only in the approximation of $\rho(T)$ for Ni.

The Debye temperatures, defined as a parameter of approximation of the $\rho(T)$ de-

pendences, are higher than those determined by other methods (see, for example, [59]). This may be due to the fact that equation (2) is a very rough approximation, in which only the scattering of electrons by longitudinal phonons is taken into account [54].

4. Conclusions

Summarizing the results obtained, we can conclude the following:

According to the results of scanning electron microscopy, for the electroconsolidated Fe–Ni composite sample, the concentration dependence of the interdiffusion coefficient of the components has a maximum at an atomic content of nickel of ~ 70 %, i.e., it is similar to the concentration dependence of the interdiffusion coefficient in Fe–Ni alloys. The value of the interdiffusion coefficient in the electroconsolidated Fe–Ni composite is significantly higher than in an alloy of a similar composition; this indicates the likely effect of the SPS technology (pressure and current along one direction during consolidation) together with the possibility of diffusion along the particle boundari es in the composite. In the samples of the equiatomic Fe–Ni system, obtained by the method of electroconsolidation, the electrical resistivity was significantly lower, and the thermal conductivity was significantly higher than in similar samples obtained by melting. The temperature dependences of the resistivity for the equiatomic system Fe–Ni and for Fe and Ni metals can be approximated with high accuracy by relations (1)–(2) over the entire temperature range of 4.2–300 K. The scattering of electrons by phonons is due to interband s–d transitions. The electron-electron scattering, as well as the scattering of electrons by spin waves, are absent. The term $\sim T^2$ in the system is caused by the interference between inelastic scattering of electrons by phonons and elastic scattering of electrons at grain boundaries and defects.

References

1. E.A.Perigo, B.Weidenfeller, P.Kollar et al., *Appl. Phys. Rev.*, **5**, 031301 (2018).
2. O.V.Dobrovolskiy, M.Huth, V.A.Shklovskij et al., *Sci. Rep.*, **7**, 13740 (2017).
3. A.L.Solovjov, E.V.Petrenko, L.V.Omelchenko et al., *Sci. Rep.*, **9**, 9274 (2019).
4. R.V.Vovk, A.L.Solovyov, *Low Temp. Phys.*, **44**, 81 (2018).
5. N.Kuganathan, A.Kordatos, M.E.Fitzpatrick et al., *Solid State Ionics*, **327**, 93 (2018).
6. R.V.Vovk, G.Ya.Khadzhai, T.A.Prikhna et al., *J. Mater. Sci.:Mater. El.*, **29**, 11478 (2018).
7. O.V.Dobrovolskiy, V.M.Bevz, M.Yu.Mikhailov et al., *Nat. Commun.*, **9**, 4927 (2018).
8. A.L.Solovjov, L.V.Omelchenko, E.V.Petrenko et al., *Sci. Rep.*, **9**, 20424 (2019).
9. M.A.Hadi, R.V.Vovk, A.Chroneos, *J. Mater. Sci.:Mater. El.*, **27**, 11925 (2016).
10. N.Kuganathan, P.Iyngaran, R.Vovk et al., *Sci. Rep.*, **9**, 4394 (2019).
11. A.Li, Z.Zhu, Y.Liu, J.Hu, *Mater. Res. Bull.*, **127**, 110845 (2020).
12. T.Nagayama, T.Yamamoto, T.Nakamura, *SID Symp. Digest Techn. Papers*, **48**, 527 (2017).
13. J.Liu, H.Liu, X.Tian et al., *J. Alloy. Comp.*, **822**, 153708 (2020).
14. T.Chen, J.Yu, C.Ma et al., *Chemosphere*, **248**, 125964 (2020).
15. N.Cai, H.Yang, X.Zhang et al., *Waste Manage.*, **109**, 119 (2020).
16. Z.Zhang, L.Cong, Z.Yu et al., *Mater. Today Ener.*, **16**, 100387 (2020).
17. Y.Wu, Y.Yi, Z.Sun et al., *Chem. Eng. J.*, **390**, 124515 (2020).
18. A.Fan, C.Qin, X.Zhang et al., *J. Mater. Chem. A*, **7**, 24347 (2019).
19. G.Zhang, G.Wang, H.Liu et al., *Nano Energy*, **43**, 359 (2018).
20. L.Ji, L.Zhang, X.Yang et al., *Dalton T.*, **49**, 4146 (2020).
21. S.Gao, H.Wang, X.Wang et al., *J. Alloy. Comp.*, 154631 (2020).
22. S.Sarkar, A.Biswas, T.Purkait et al., *Inorg. Chem.*, **59**, 5194 (2020).
23. X.Zhu, D.Zhang, C.J.Chen et al., *Nano Energy*, **71**, 104597 (2020).
24. S.Goto, H.Kura, E.Watanabe et al., *Sci. Rep.*, **7**, 1 (2017).
25. V.L.Kurichenko, D.Y.Karpenkov, A.Y.Karpenkov et al., *J. Magn. Magn. Mater.*, **470**, 33 (2019).
26. F.Bernard, S.Le Gallet, N.Spinassou et al., *Sci. Sinter.*, **36**, 155 (2004).
27. V.V.Skorokhod, A.V.Ragulya, *Poroshkovaya Metallurgiya*, **3–4**, 3 (1994).
28. D.L.Bourell, J.R.Groza, *Powder Metallurgy. ASM Handbook*, **7**, 504 (1998).
29. Ya.E.Geguzin, Sintering Physics, 2-nd ed., Nauka, Moscow (1984) [in Russian].
30. V.Y.Kodash, J.R.Groza, K.C.Cho et al., *Mat. Sci. Eng. A*, **385**, 367 (2004).
31. E.Aslan, N.Camuscu, B.Birgoren, *Mater. Design.* **28**, 1618 (2007).
32. B.S.Bokshtejn, Diffusion in Metals, Metallurgiya, Moscow (1978) [in Russian].
33. A.Kohn, J.Levasseur, J.Philibert et al., *Acta Met.*, **18**, 163 (1970).
34. Yu.E.Ugaste, A.A.Kodentsov, F.Van Loo, The Phys. *Metals. Metallog.*, **88**, 88 (1999).
35. M.Badia, Interdiffusion of Fe and the Transition Metals, Ph.D. Thesis, Univ. Nancy, France (1969).

36. J.I.Goldstein, R.E.Hanneman, R.E.Ogilvie, *Trans. Metall. Soc. AMIEV*, **233**, 812 (1965).
37. R.Berman, Thermal Conduction of Solids, Clarendon Press, Oxford (1976).
38. C.Y.Ho et al., *J. Phys. Chem. Ref. Data*, **12**, 183 (1983).
39. C.Y.Ho, M.W.Ackerman, K.Y.Wu et al., *J. Phys. Chem. Ref. Data*, **7**, 959 (1978).
40. A.M.Ermolaev, B.A.Merisov, V.I.Khotkevich, *Fizika Metalov i Metallov.*, **24**, 1104 (1967).
41. B.A.Merisov, G.Ya.Khadzhaj, P.N.V'yugov et al., *Metallofiz. Noveishie Tekhnol.*, **33**, 301 (2011).
42. V.A.Pervakov, Low-temperature Thermal Conductivity of Metals with Defects, Gos. Spez. .Izd. Osnova, Kharkov (1993) [in Russian].
43. Yu.Kagan, A.P.Zhernov, *Zh. Eksper. Teor. Fiziki*, **50**, 1107 (1966)
44. A.M.Ermolaev, *FMM*, **23**, 813 (1967).
45. K.Jin, B.Sales, G.Stocks et al., *Sci. Rep.*, **6**, 20159 (2016).
46. P.L.Rossiter, The Electrical Resistivity of Metals and Alloys, Cambridge University Press (1987).
47. Z.Hashin, S.Shtrikman, *J. Appl. Phys.*, **33**, 3125 (1962).
48. A.H.Wilson, *Proc. Roy. Soc. A*, **167**, 580 (1938).
49. L.Colquitt, *J. App. Phys.*, **36**, 8 (1965).
50. G.W.Webb, *Phys. Rev.*, **181**, 1127 (1969).
51. S.Banerjee, A.K.Raychaudhuri, *Phys. Rev. B*, **50**, 8195 (1994).
52. Y.Kao et al., *J. Alloy. Comp.*, **509**, 1607 (2011).
53. O.A.Gavrenko, B.A.Merisov, G.Ya.Khadzhaj, *Met. Phys. Adv. Tech.*, **15**, 1215 (1996).
54. J.M.Ziman. Electrons and Phonons. The Theory of Transport Phenomena in Solids, Oxford at the Clarendon Press (1960).
55. N.V.Volkenshtein, V.P.Dyakina, V.E.Startsev, *Phys. Stat. Sol. B*, **57**, 9 (1973).
56. J.-F.Lin, J.P.Bird, L.Rotkina et al., *App. Phys. Lett.*, **84**, 3828 (2004).
57. S.S.Yeh, J.J.Lin, Jing Xiunian et al., *Phys. Rev. B*, **72**, 024204 (2005).
58. M.Yu.Reizer, A.V.Sergeev, *Zh. Eksper. Teor. Fiziki*, **65**, 1291 (1987).
59. Y.Tanji, *J. Phys. Soc. Jpn.*, **30**, 133 (1971).